Environmental Science Nano

# Exploring the Properties and Applications of Nanoceria: Is There Still Plenty of Room at the Bottom?



| | |
|---|---|
| Journal: | *Environmental Science: Nano* |
| Manuscript ID: | EN-PER-05-2014-000079.R3 |
| Article Type: | Tutorial Review |
| Date Submitted by the Author: | 28-Aug-2014 |





| | |
|---|---|
| Complete List of Authors: | Reed, Kenneth; Cerion NRx,<br>Cormack, A; Alfred University, School of Ceramic Engineering and Materials Science<br>Kulkarni, Aniruddha; CSIRO, Energy Technology<br>Mayton, Mark; Spinnaker Cross, Inc.,<br>Sayle, Dean; Kent University, SPS<br>Klaessig, Fred; Pennsylvania Bio Nano Systems,<br>Stadler, Bradford; Cerion NRx, |

## Nano impact statement

This article is one in a series of papers covering the unique properties and usages of nanoceria, as discussed at the Nanoceria Workshop associated with the Sustainable Nanotechnology Organization's 2nd Annual Conference in November of 2013. The dedication of a full day Workshop to nanoceria's prospects speaks to the impact and potential of this specific form of nanotechnology. This introductory review functions as a primer for the topics described in greater detail in the subsequent papers. Particular attention is given to the potent redox properties of the material, borne of its electronic, chemical, and physical nature, as well as its uses and in current and future commercial and therapeutic applications.

Environmental Sciences: Nano RSCPublishing

ARTICLE

# Exploring the Properties and Applications of Nanoceria: Is There Still Plenty of Room at the Bottom?

Cite this: DOI: 10.1039/x0xx00000x

Kenneth Reed,[a] Alastair Cormack,[b] Aniruddha Kulkarni,[c] Mark Mayton,[d] Dean Sayle,[e] Fred Klaessig,[f] and Brad Stadler [a]

Received 00th January 2012,
Accepted 00th January 2012

DOI: 10.1039/x0xx00000x

www.rsc.org/

Nanoceria is an exceptionally versatile, commercially valuable catalytic material whose properties vary dramatically from that of the bulk material. Nanoceria's redox properties can be tuned by choice of method of preparation, particle size, nature and level of dopant, particle shape and surface chemistry. The two oxidation states of the cerium element in the lattice make possible the formation of oxygen vacancies which are essential to the high reactivity of the material, its oxygen buffering capability and thus its ability to act as a catalyst for both oxidation and reduction reactions. Ceria has important commercial utility in the areas of chemical mechanical polishing and planarization, catalytic converters and diesel oxidation catalysts, intermediate temperature solid oxide fuel cells and sensors. Its potential future uses include chemical looping combustion, photolytic and thermolytic water splitting for hydrogen production and as a therapeutic agent for the treatment of certain human diseases. We have seen that the method of synthesis, particle size, stabilizing corona, and purity dictate where it is used commercially. Finally, in regards to the prescient words of Dr. Feynman, we note that while there is indeed "plenty of room at the bottom", there quite possibly exists an optimal nanoceria size of between 2-3 nm that provides maximal reactivity and thermodynamic stability.

## Introduction

In this, the introductory article from the Sustainable Nanotechnology Organization (SNO)-sponsored ceria workshop, we review the chemistry and applications of nanoscale cerium oxide, nanoceria, for a broad scientific audience, identify the current knowledge state and knowledge gaps and make recommendations for future research.

We first discuss the element cerium, its atomic structures and natural abundance and then progress to the solid-state nature of cerium dioxide, ceria, as crystalline nano-particles. Properties of nanoceria, including its electrochemistry, formation of nanoparticles, and self-assembly into various morphologies are addressed with emphasis on the dominating influence of oxygen vacancies in ceria chemistry. Select commercially important applications are presented along with some very promising future energy and biochemical/health related applications.

Elements of this paper serve as an overview for the subsequent papers of this series. The examples given are intended to be exemplary and not exhaustive although when available, recent review articles on each specific subject are cited.

## Cerium and Cerium Dioxide (Ceria)

The element cerium (atomic number 58), the second member of the lanthanide series or rare earth elements, is, paradoxically, not particularly rare in abundance in the earth's crust. It is the most abundant element of the rare earth family, approaching levels of the major industrial metals Ni, Cu and Zn [1 2 3].

Cerium is the first element in the periodic table to posses a ground state electron in a 4f orbital (Xe $4f^1 5d^1 6s^2$), which is responsible for its powerful reduction/oxidation (redox) behaviour when cycling between its two ionic states, the ceric ion, $Ce^{+4}$ (the Xe ground state), and the cerous ion, $Ce^{3+}$ (Xe $4f^1$). As one might expect, the more highly oxidized state has a smaller ionic radius, 97 pm, versus 114 pm. Perhaps somewhat unexpectedly, the much lighter oxygen di-anion in the ceria lattice is much larger in ionic radius, 135 pm, than even the $Ce^{3+}$ cerium ion [4].

This cycling between two electronic states differing only by one 4f electron defines the cerium ion Nernstian behaviour in liquids, $Ce4^+ + 1\ e^- \rightarrow Ce^{3+}$:

Equation 1. $E = 1.44 - 0.059\ \mathrm{Log}\ [Ce^{3+}]/[Ce^{4+}]$

The electrochemical potential of this reduction reaction is modulated quite strongly by the attendant solvent phase (1.44 V for sulfuric acid but 1.70 V for perchloric acid) and also by the counter (or gegen) ion both for aqueous and non-aqueous media. For example, the cerium perchlorate $Ce^{3+}/Ce^{4+}$ $E^0$ potential is 1.7 V while the carbonate potential is ~0.7 V (all vs. saturated calomel electrode) [5]. The review by Grulke and colleagues in this themed collection provides a much more detailed description (using Pourbaix diagrams) of the aqueous cerium ion chemistry and hydroxyl species phase equilibrium as a function of pH and electrochemical potential [114].

These dramatic $E^0$ behavioural excursions take on additional significance for the nano-scale crystal where the surface-terminated cerium ion's 8-fold coordination may only be partially compensated (4-fold or less depending upon lattice position) by adsorption of various solute molecules.

Turning now to the ceria crystal itself, we observe that each cerium atom is bonded to eight oxygen atoms (eight–fold coordinated), while each oxygen atom is four-fold coordinated (Fig. 1). The complete unit cell, $Ce_4O_8$ measures 0.51 nm (5.1 Å) on an edge, and is a face-centered cubic (fcc) fluorite lattice [6].

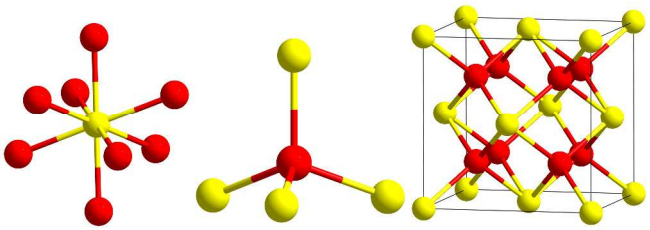

(a) (b) (c)

Figure 1. Structural analysis of ceria crystals and unit cells. Eight-fold coordinated cerium atoms (yellow) with four-fold coordinated oxygen atoms (red) in ceria crystals (a and b) and the primitive unit cell (c). Figure kindly provide by Alastair Cormack.

Depending upon the synthesis conditions, Crystallites can be comprised of several or many unit cells. For example, a 1.1 nm particle, the smallest ceria nanoparticle theoretically possible7 would contain 8 unit cells (2x2x2)[7]. The assessment of crystallite size is usually performed by analysis of an x-ray diffractogram and the use of the Scherrer equation [8].

Crystallites are the elementary building blocks for nanoparticles in general. Nano-particles and nanoceria can be either mono-or polycrystalline with the latter being more common. This leads to several descriptions of particle size, based upon the analytical method employed. X-ray diffraction (XRD) techniques can be utilized to determine crystallite size, while transmission electron microscopy (TEM) can determine nanoparticle shape and constituent particle size. Finally, to determine the hydrodynamic size (particle size with its attendant adsorbate and solvation sphere), dynamic light scattering techniques (DLS or photon correlation spectroscopy)[9] are employed. It is instructive to compare TEM geometric size to XRD crystallite size to obtain an estimate of the number of crystallites per particle. Commonly, nanoparticles are composed of a plurality of crystallites, but we will give an interesting nanoceria example of a single crystallite per particle in the synthetic methods section.

This hierarchal assembly of unit cells into crystallites and crystallites into particles can be extended even further by self-assembly (oriented attachment at particular surfaces) [10] of particles into larger structures, such as rods, sheets, cubes and hollow or porous variants, which can vary in size within the 1-100 nm range (Fig. 2). Additional polymorphs, such as nanowires, nanocubes, hollow plates, and tabular triangular grains have also been synthesized [11-13].

Often, molecular dynamics simulations involving simulated crystallisation and self-assembly can provide insight into the resultant geometry and formation of these structures. These theoretical models can then be interrogated to predict a variety of properties such as crystal strain. Crystal strain is the displacement of atoms from their equilibrium lattice positions that results in particle energy in excess of the equilibrium value. This strain energy can be exploited to modulate chemical reactivity (strain-tuneable reactivity) [14]. The unique chemistry and commercial potential of these novel structures is an active area of research and development.

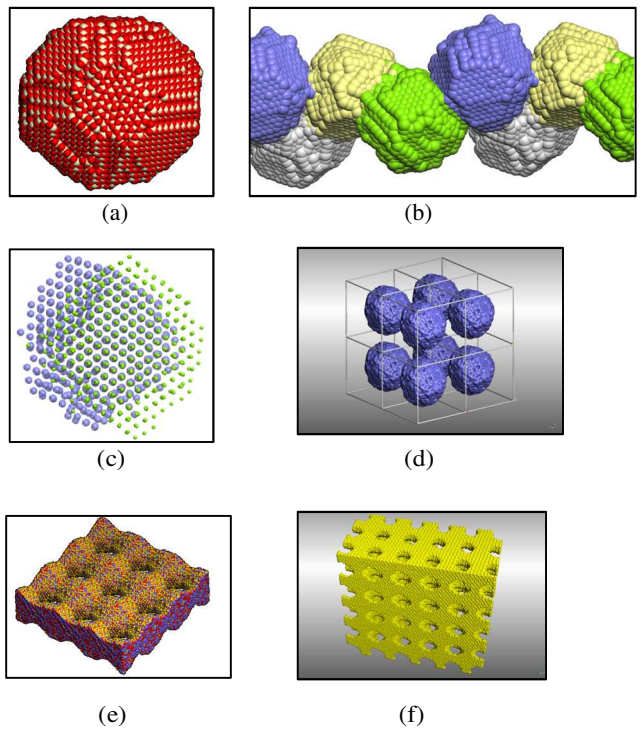

(a) (b) (c) (d) (e) (f)

Figure 2. Self-assembly and oriented attachment of ceria nanoparticles into various architectures: (a) ceria nanoparticle, (b) ceria nanoparticles agglomerate together to form a nano-rod, (c) oriented attachment of the faces of the nanoparticles, (d) assembly into a periodic cubic array, (e) formation of nano-sheets, and (f) mesoporous (larger micro scale and open) architectures.

Permissions: (a) Reproduced by permission [15], The Royal Society of Chemistry copyright 2012. (b,c) reproduced with permission [16]: (d,f) reproduced with permission from: [17]

## Nanoceria Properties

### Oxygen Vacancy

The concept of the oxygen vacancy is that of a missing oxygen atom (or atoms for a di or tri vacancy) in one or more of the eight octants in a ceria unit cell [6, 18, 19]. This is conceptually straightforward to visualize in atomic models (Fig 3).

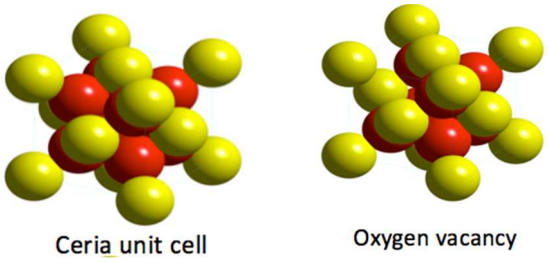


(a) (b)

Figure 3. Ceria unit cell (a) and a unit cell with a single oxygen vacancy (b) wherein one oxygen atom is missing from the uppermost left and forward octant position. Figure kindly provide by Alastair Cormack.

Perhaps one of the most visually compelling demonstrations of the presence of oxygen vacancies and the clustering of oxygen vacancies is the elegant high vacuum work of Esch and co-workers [20] who used scanning tunnelling microscopy coupled with density functional calculations of the local surface structure on an oriented ceria crystal to reveal surface and subsurface oxygen vacancies generated at 900°C. As electronic charge is conserved, a single oxygen vacancy must be offset by the reduction of two $Ce^{4+}$ atoms. The location of the resulting two $Ce^{3+}$ atoms, be they adjacent (called a triplet) or remote from the oxygen vacancy, is currently a matter of debate and may very well depend upon the size, form and manner of synthesis of the ceria crystal. Additionally, different analytical methods used to assess the $Ce^{3+}$ concentration yield conflicting results. In the examination of 3 nm nanoceria, Dutta and colleagues [21] found a value for this concentration of 18% based upon electron magnetic resonance (EMR) and magnetization measurements. High vacuum TEM-derived results of Seal and colleagues provide a value of 44% at this particle size [22]. In contrast, Cafun and colleagues [23] who used high energy resolution hard X-ray spectroscopy to directly probe the Ce 4f orbitals believe, at this particle size, that the picture is more like an "electron sponge" in which the electron density is not localized to a given set of atoms but is spread out over the entire crystal structure. Bond lengthening in which extra electrons populate orbitals accommodates electron density that arises from Ce-O orbital mixing (i.e. there is no localized reduction of surface $Ce^{4+}$ to $Ce^{3+}$). While the question of cerium atom charge and association with oxygen vacancies remains unresolved, it is generally agreed that the percentage of cerium atoms in the reduced state increases with decreasing particle size. Using high resolution TEM, Seal and colleagues [22] calculated an increase in $Ce^{3+}$ concentration from 17 to 44% as particle size decreased from 30 to 3 nm.

The existence of nanoceria oxygen vacancies with or without attendant localized $Ce^{+3}$ atoms is not confined to high vacuum, high temperature conditions. Muller and colleagues [24] have utilized TEM and Electron Energy Loss Spectra (EELS) on aqueous-synthesized 2 nm ceria particles to demonstrate localization of the reduced cerium atoms to the particle surface (Fig. 4).

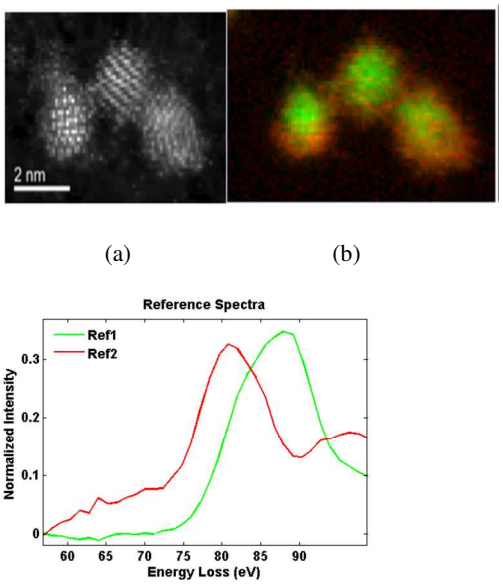


(a) (b)

(c)

Figure 4. An ultra high resolution TEM and EELS study of selected nanoceria particles. Annular dark field image (a), their oxidation state map (b) with $Ce^{+3}$ false colored red, $Ce^{+4}$ green (b) and the associated EELS spectrum (c)[24].

The Ce□edge of the normalized EELS intensity curve shifts to lower energies on the surface of the Ce□rich particles (red curve labelled Ref2 vs. green curve labelled Ref 1 in Fig. 4c), suggesting a reduction of the Ce valence on the surface of the particles. This may result from less constraint of cerium's ionic radius when it is located on the surface and not in the particle core.

While it may be instructive to measure the $Ce^{3+}/Ce^{4+}$ ratio to learn about the oxygen vacancy concentration, the oxygen vacancy construct itself can actually be quantified by a number called the oxygen storage capacity (OSC). This number is expressed as micromoles of oxygen liberated per gram of starting material. The OSC for molecular cerium dioxide (gas phase) is 1452.47 μ moles O2/g and is described by the following equilibrium process:

Equation 2. $CeO_2 \leftarrow \rightarrow CeO_{2-x} + x/2\ O_2 \quad x = 0.5 \quad CeO_{1.5}\ (Ce_2O_3)$

Since commonly used ceria is produced as micro- or nano-scale crystals and not as a gas phase molecule, the fully reduced commercial ceria may only approach a fraction of the theoretically calculated OSC in equation 2. This equation implies a reversible

reaction, an idea that is fundamental to the performance of a material as a catalyst. Indeed, solid particle ceria can be thought of as an "oxygen buffer" [6] that either provides or removes oxygen to/from the surrounding environment by responding to a lack or excess of oxygen in that environment. The ability to reversibly extract oxygen atoms from the lattice has obvious utility for the catalytic oxidation of various materials such as carbon monoxide, soot, and other partially oxidized exhaust gases (Fig. 5)

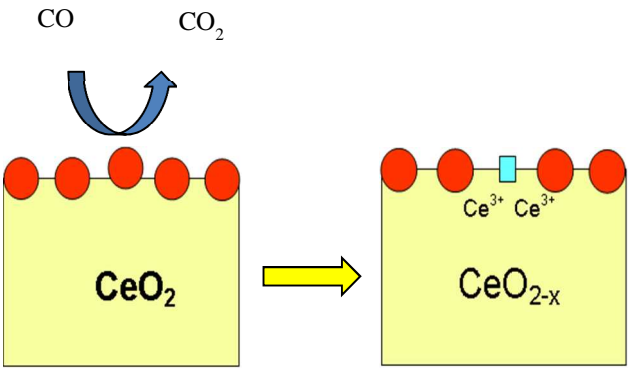


Figure 5. A $CeO_2$ particle creating an oxygen vacancy while oxidizing carbon monoxide to carbon dioxide and simultaneously reducing two $Ce^{4+}$ atoms. Figure kindly provided by Aniruddha Kulkarni.

Further utilizing the OSC concept to quantify oxygen vacancy formation, one can generate reactivity maps or fingerprints of the regions of highest (easy to extract oxygen) and lowest (difficult to extract oxygen) surface reactivity (Fig. 6).

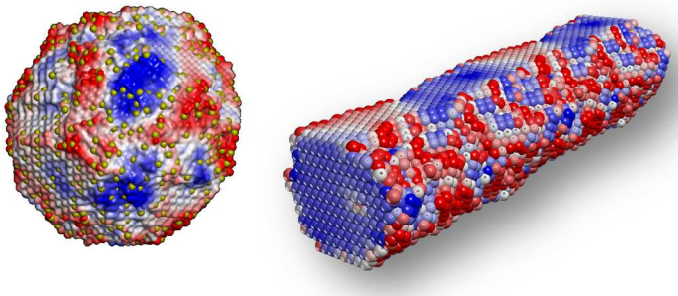

Figure 6. Reactivity 'fingerprints' of (a) ceria nanoparticle, and (b) ceria nanorod. Regions colored red indicate high reactivity and regions colored blue indicate low reactivity. The yellow spheres in (a) are $Ce^{3+}$ ions. Reproduced with permission [15]: The Royal Society of Chemistry copyright 2012.

Accordingly, atomistic simulation can also predict the topographical factors influencing surface activity. For example, steps, edges and corners are generally more reactive than flat feature less planes. The activity also depends upon microstructure and strain in the nanocrystals.

**Nanoceria Size Effects**

In addtion to topographical features, nanoparticle size is also a critical parameter in determining particle reactivity. Unlike most nano-structures, nanoceria is unique in that the lattice expands as the particle becomes smaller. This lattice expansion leads to a decrease in oxygen release and reabsorbtion. In a careful electron diffraction study of a nanoceria particle size series from 11.8 nm to 1.1 nm, Hailstone and colleagues [7] found a sytematic lattice expansion increase over that of bulk ceria. This increase was only 1.1% for the 11.8 nm particle but increased dramatically to 6.8% for the 1.1 nm particle. In absolute values, the lattice constant of the smallest particle size was 4.056 Å. For comparison, the lattice constant of bulk ceria is 3.825 Å. The author's interpretation of this phenomenon is that at 1.1 nm, a large fraction of the cerium atoms are in the fully reduced state, even though the ceria nanoparticles retain a cubic lattice, and not the predicted hexagonal lattice (Fig. 7).

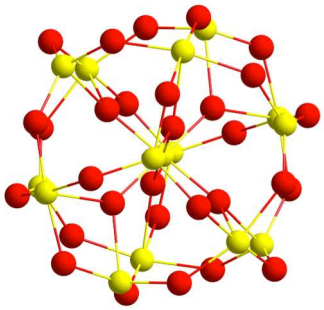

Figure 7. Two superimposed 1.1 nm ceria particles, one with and one without the associated lattice expansion. Oxygen atoms= red, cerium= yellow. Figure kindly provide by Alastair Cormack.

Supporting the idea that the 1.1 nm nanoceria particle is nearly fully reduced is the observed OSC calculation of only 65 µmol $O_2$/g . This OSC value represents a major reduction from the 425 µmol $O_2$/g value of the 11.8 nm particle, and similarly from that of bulk ceria (296 µmol $O_2$/g).

The work of Hailstone and colleagues [7] suggests that there may be a nanoceria size, of 2-3 nm, that provides the maximum OSC value. This suggests that the familiar curve showing nanoparticle reactivity increasing monotonically towards smaller dimensions may actually peak in the 2-3 nm range. This size would correspond approximately to a $Ce_{80}O_{160}$ particle. Indeed, density functional calculations by Migani and colleagues [25] on a size series of $CeO_2$ units revealed that as the particle size increased, the oxygen vacancy formation energy requirement decreased dramatically. For $C_{40}O_{80}$ the vacancy energy requirement was found to be 0.8 eV while for $Ce_{80}O_{160}$, it is only 0.46 eV. Additionally, the removal of the lowest coordination number oxygen atoms, which are only bonded to two adjacent cerium atoms, required the lowest calculated energy.

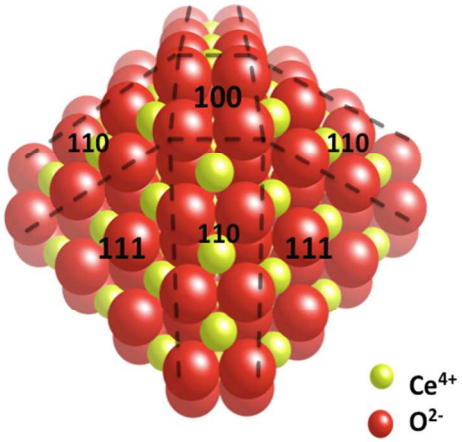


Figure 8. An atomistic depiction of a 2 nm, surface-terminated, $C_{80}O_{160}$ particle with the appropriately labelled Miller indices. Figure kindly provide by Alastair Cormack.

At this 2 nm size, the 24 corner atoms, which are labelled by their Miller index position, {100} in Fig. 8. are only two and not four coordinated to adjacent cerium atoms and are therefore quite labile. Experimental support for these preferred {100} reactive sites can be found in the work of Zhang and colleagues on cubic (i.e. {100}) face) nanoceria crystals [26]. They observe an appreciable OSC at 150°C. This low temperature OSC is approximately 250°C lower than that of irregularly shaped nanoceria that do not possess these unique lattice positioned, labile, oxygen atoms.

Previously, we noted that the *in vacuo* estimates for the $Ce^{3+}$ ion concentration ranged from 18 to 44%. Further insight into the $Ce^{3+}$ ion concentration question in nanoceria in this size regime can be obtained by focusing on the most labile oxygen atoms in the {100} lattice sites. Notice that there are six corners to the nanoceria structure in Fig. 8, which are composed of a quartet of these particular atoms. If only one atom from each site contributed to the measured OSC, this would result in twelve reduced cerium atoms. The resultant $Ce^{3+}$ concentration would then be 12/80 or 15% and the (calculated) OSC would be 436.1 µmole/gm. affording $CeO_{1.85}$. Alternatively, using Hailstone's reported OSC value of 349 µmole/gm, we derive a formula for reduced ceria, $CeO_{1.875}$ that would require a $Ce^{3+}$ ion concentration of 25%. Thus the lower $Ce^{3+}$ concentration estimate provided experimentally by electron magnetic resonance studies appears more reasonable and the *in vacuo*, high beam energy TEM and UPS studies appear to overestimate this value as has been previously noted.[27]

Finally, we note that vacancy formation from these 24 atoms would produce $CeO_{1.7}$ (and not $CeO_{1.5}$) as the lower practical limit, with an inherent OSC of 872.1 µmol $O_2$/g. Since Hailstone and colleagues observed an OSC of only 349, then not all of the most labile corner atoms have contributed to the oxygen vacancy population. It appears that the OSC at this size is not limited by oxygen atom availability but perhaps by other factors such as the ability to accommodate only a certain number of reduced cerium atoms or co-located vacancies or perhaps energetics of formation of twelve vacancies.

**Lattice Doping**

One of the more powerful ways of modulating ceria's oxygen vacancy defect concentration, and hence particle reactivity, is the doping of foreign metals into the cerium atom sub-lattice. In these cases, the cerium atoms can be replaced with di- or tri-valent transition metals or other lanthanides. Structurally, this is represented in the accompanying 2 nm atomistic model (Fig. 9).

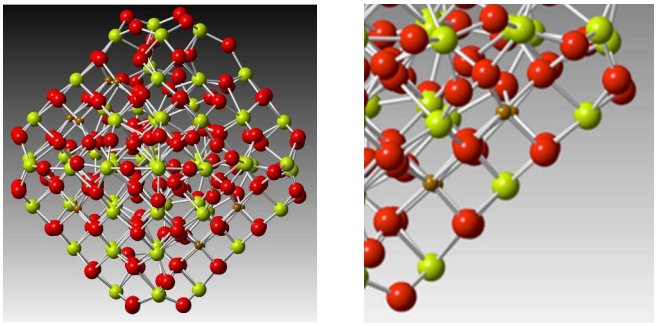

Figure 9. Atomistic model representing doping of the ceria sub-lattice with metal ions. A 2 nm doped ceria nanoparticle (full, a, and expanded view, b) with the smaller dopant atom (brown) substituting for a cerium ion (yellow-green) in the lattice. Oxygen atoms= red. Figure kindly provide by Alastair Cormack.

Sauer and colleagues [28] have recently provided a comprehensive review of oxygen defects in ceria comparing quantum chemical and experimental studies. Included in this study are examples of transition and lanthanide metal doping into ceria lattices. Interestingly, they report for the case of La ion doping that the calculated oxygen vacancy formation energies are about 2 and 1.7 eV smaller for the {111} and {110} surfaces, respectively. Babu and colleagues [29] studied the influence of doping micro-emulsion-based ceria nanoparticles with Sm, Gd, Y, and Yb. The anticipated effect was that both $Ce^{3+}$ atom and oxygen vacancy concentration should increase, but unexpectedly, they found that nanoceria doped with the smallest atomic radius ion, Yb, demonstrated decreased $Ce^{3+}$ and oxygen vacancy concentration.

The literature focused on modifying nanoceria properties with the use of metal ion dopants is quite extensive. The reader should examine critically whether the full suite of evidence has been brought forth to firmly establish dopant incorporation and amounts within the lattice. These analytical techniques should include, but are not necessarily limited to; TEM, selective area electron diffraction (SAED), inductively coupled mass spectrometry (ICP-MS), specific surface area and of course XRD.

The effects of divalent ion doping on the $Ce^{3+}$ and oxygen vacancy concentration can be understood by considering that when one rare earth oxide ($Re_2O_3$) replaces two $CeO_2$ units, an additional two electrons are required to maintain nanoparticle charge neutrality. This follows because the Re ion is in a +3 state and cerium is in a +4 state. The required electrons are provided by forming an oxygen vacancy with the attendant reduction of two $Ce^{4+}$ atoms to $Ce^{3+}$.

Exactly which cations can be doped into a ceria lattice? It would be tempting to assume that cations with ionic radii less than that of the cerium ion would be ideal dopant candidates although this is not always the case. The energetics (enthalpy) of dopant incorporation (thermodynamic allowance) must be taken into account. Here, modern computational quantum mechanical techniques provide some guidance. The group of Alistair Cormack [30] has calculated that the substitution of the much smaller iron atom (78 pm) for cerium (97 pm) is endothermic (not favored) by 4.322 eV per $Fe_2O_3$ unit. Interestingly, in the case of lanthanum (116 pm), the substitution is exothermic by 3.313 eV per $La_2O_3$.

Support for the Cormack group dopant calculations comes from work by Muller and colleagues at Cornell and Hailstone at Rochester Institute of Technology [24], who use both TEM and EELS to demonstrate poor iron incorporation into a 2 nm ceria nanoparticle (Fig. 10). It would appear that the iron has preferentially formed a shell partially surrounding the particle.

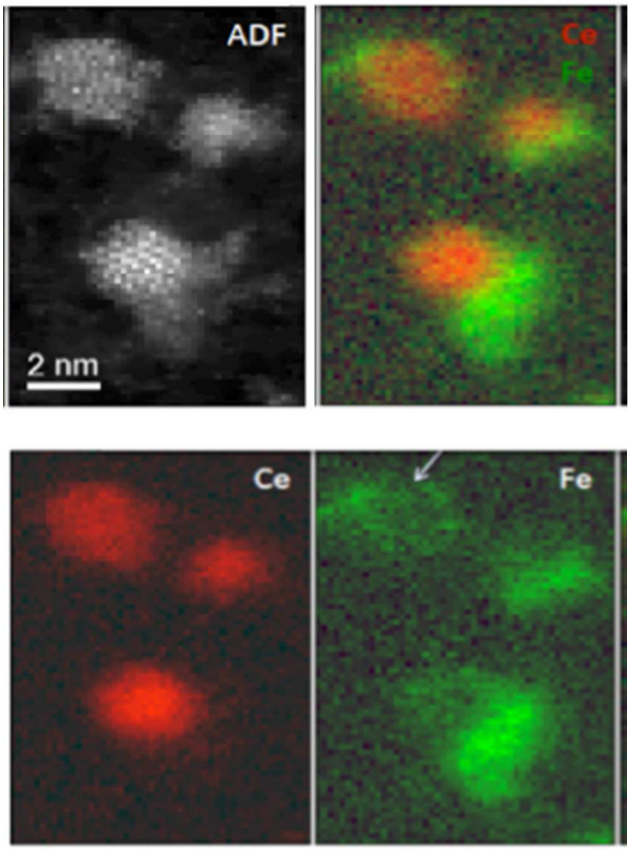


Figure 10. Annular Dark Field (ADF) of three nanoceria crystals. Top right is the combined Ce and Fe elemental maps with the separate Fe (false colored green) and Cerium (false colored red) elemental maps below[24].

Additionally, the work of Hailstone and colleagues [31] showing iron incorporation extending up to 59%, provided XRD data showing very little perturbation in the scattering angle positions of the XRD peaks (called Bragg reflection angles) in the doped ceria. These peaks should have differed from the undoped ceria if iron incorporation had actually occurred. These results all support the idea that very little doped iron is incorporated (estimated 2-4 %) into the ceria lattice under low temperature conditions and the associated iron is in an amorphous state.

## SYNTHETIC METHODS

In light of ceria's complex physical and interesting properties, it is perhaps not surprising that numerous methods have been developed to synthesize these materials. We will describe several important synthetic methods, and the reader is referred to a recent excellent review article on this topic [32].

Broadly speaking these synthetic methods can be partitioned into two temperature regimes; lower temperatures here defined as (<250°C) and higher temperature regimes that can extend to combustion, flame synthesis and even plasma arc temperatures that can reach several thousand degrees centigrade.

The most numerous and commonly employed lower temperature wet-chemical synthetic methods for the production of nanoceria are: co-precipitation [33 34], hydrothermal [35, 36 37], solvothermal [38 39], [40], sol-gel [41 42], Pechini [43] (a modified sol-gel method using citric acid), micro emulsion and reversed micelle methods [44 45],[46 22 47]. These methods are favored for small scale and research quantities of materials.

Typically these techniques rely on a source of $Ce^{+3}$ and an oxidant to convert the cerous ion to the more insoluble ceric $Ce^{4+}$ ion, and one or more stabilizers, which may also play the dual role of both stabilizer and oxidizer. The formation of nanoceria under these conditions follows the classical LaMer/Dinegar mechanism [48] in which the solution first becomes supersaturated in cerium ion after a short nucleation burst (the supersaturated state exceeds the thermodynamically stable limiting concentration of ions) followed by the subsequent collapse of the supersaturated state to produce particles. If no further (re-) nucleation occurs, the particles can be uniform in size frequency distribution and may subsequently grow in size. The final particle size is controlled by the concentration and binding strength of the adsorbed stabilizer (s) which regulate the total molar surface area that is thermodynamically stable for a given set of experimental conditions. The suite of stabilizers are many and varied but those most commonly used include: organic alcohols [49], polymers such as poly vinyl pyrrolidone [50], and carboxylates [51 52 53]. Organic amines such as oleylamine have been used by Colvin [54] and co-workers at Rice University to construct a "library" of ceria

nanocrystals from 3-10 nm for biological applications using high temperature thermal decomposition techniques.

Homo and co-precipitation reactions already mentioned, while useful for the production of nanoceria, require subsequent washing and re-suspension. It is possible to form thermodynamically stable nanoceria colloids directly without a separate isolation step. Consider the following example of such a reaction, additionally, one that has been scaled to large production volumes by Cerion Advanced Materials (Rochester, NY) [55]. (Scale-up was a concern raised at the SNO sponsored nanoceria conference limiting the widespread adoption of nanotechnology). A low temperature-synthesized nanoceria colloid is formed under hydrothermal, 80 °C, reaction conditions at ambient atmospheric pressure. Two stabilization chemistries, citric acid and EDTA, are employed to produce a crystalline, ceramic ceria nanoparticle [51]. In Eq. 3., cerium hydroxide is formed from a soluble cerium salt and ammonia, while the hydroxide that is subsequently produced is oxidized to the oxide by a suitable oxidant (hydrogen peroxide) in Eq. 4:

Equation 3. $Ce(NO_3)_3(6H_2O) + 2NH_4OH \rightarrow$

$2NH_4NO_3 + 6H_2O + Ce(OH)_2NO_3$

Equation 4. $2Ce(OH)_2NO_3 + H_2O_2 \rightarrow 2CeO_2 + 2H_2O + 2HNO_3$

As seen in the 250,000x TEM (Fig. 11), un-agglomerated nanoparticles result whose population is uniform in particle size frequency distribution. The physical dimensions are 3 nm with a coefficient of variation of 10%. The XRD pattern demonstrates that the nanoceria is crystalline in nature. This specific nanoceria composition was further discussed at the SNO Workshop in the context of ceria as a therapeutic drug.

Both the crystallite and particle size are identical, which is atypical in these reactions and thus one can make the inference that each particle is composed of a single crystallite (on average). Furthermore, if we assume a 0.519 nm edge length per crystallite then the average particle is composed of about six unit cells (on edge dimension).

From the previous discussion on the size dependent behaviour of oxygen vacancy formation, and the decrease in OSC at ~ 1nm, we conclude that these nanoceria may lie at the threshold of optimal reactivity, that being the size of maximal OSC and reactivity. This conclusion may have rather interesting implications for Richard Feynman's statement that "there is plenty of room at the bottom". [56]

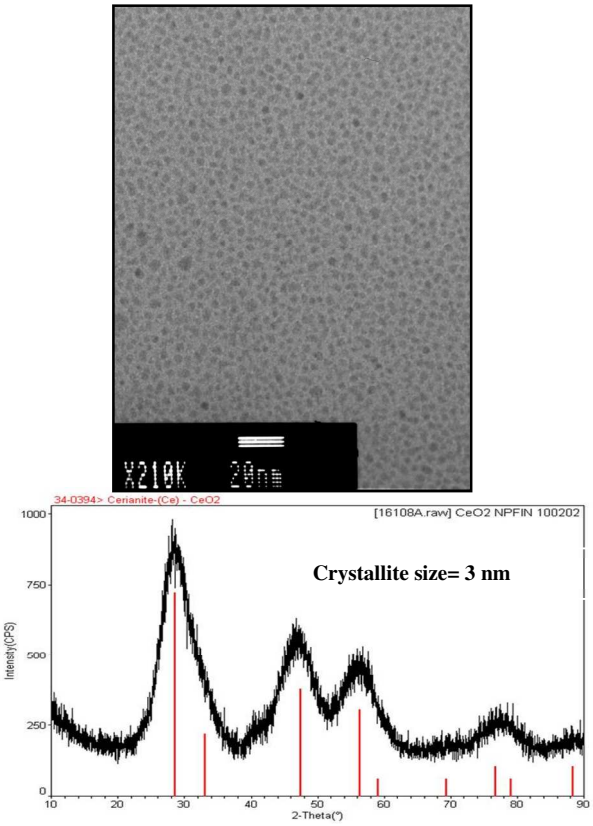


Figure 11. TEM and XRD of a 3 nm crystalline nanoceria dispersion made according to Equations 3 and 4. Figure kindly provided by Rich Hailstone.

Higher temperature processes for the production of ceria and doped ceria composition, such as the aerosol processes, can operate at very high combustion temperatures, 1000 to 2500°C. These processes employ ceria precursors such as cerium alkoxide or carboxylate aerosols that are fed into a reaction chamber in a continuous manner. Physical vapor synthesis represents another technique (NanoPhase Corporation and the NanoARC process) utilizes an argon plasma arc operating at several thousand degrees centigrade.

At these very high temperatures, the direct synthesis of ceria provides very prismatic (i.e. sharp edges and corners), five to several thousand nm agglomerates. These stand in marked contrast to the particle morphologies produced at temperatures < 250 °C, more commonly < 100 °C where well-differentiated sub 5 nm spherical and star-like nanoparticles can be made [57].

Calcination is a commonly employed high temperature technique for the industrial scale production of ceria in which the as-made cerium composition is not yet an oxide. This process involves high temperature treatment below the melting point of the material in an oxygen atmosphere. Table 1. Contains several important industrial ceria manufacturers and their processes for the production of ceria.

Table 1. Selected large industrial firms and their ceria production processes

| Firm | Likely Process |
|---|---|
| Hitachi | Precipitation (carbonate chemistry prominent); then calcined and milled [58] |
| Rhodia | Precipitation (hydroxide chemistry prominent); then calcined and milled [59] |
| Antaria | Precipitation while being mechanically milled in a NaCl media [60] |
| Umicore | Precipitation while being evaporated (thermal spray) [61] |
| Evonik | Pyrogenic gas phase formation from metal-alkoxides or metal- carboxylates [62] |

Unlike the LaMer/Dinegar mechanism previously described for particle size control, for both the Umicore and Evonik processes, particle size is controlled by gas phase temperature and velocity conditions.

In discussing the role of ceria additives, it is useful to analogize the various sulfate titania processes. Manufacture of titania from the sulfate process involves precipitation from metatitanic acid using recycled seed crystals (rutile or anatase). Additionally, phosphate is added prior to calcination for both particle size control and to minimize sintering during calcination. Aluminum salts added as a surface treatment, is known to promote needle-shaped crystals [63].

Similar uses of process additives are possible in commercial $CeO_2$ samples. More specific to nanoceria is the recent proposal [57] that process temperatures can influence biological activity acting either as an antioxidant or pro-oxidant. Additionally, investigators are strongly advised to conduct simple characterization tests: thermal gravimetric analysis (TGA); loss on drying (LOD); loss on ignition (LOI); and point of zero charge testing to ensure that the particle examined matches their expectations as to surface chemistry.

## Selected Important Commercial Applications

In this section we discuss some of the more widely known applications of ceria and nanoceria including large industrial and commercial applications: CMP processes (chemical mechanical polishing for optical elements, and chemical mechanical planarization for semi-conductor wafers), industrial catalysis, catalytic converters, fuel additives, fuel cells and other electrochemical devices and some more common everyday household instances in which we encounter ceria.

### CMP (Chemical Mechanical Polishing and Planarization

The purpose of chemical mechanical polishing of optical elements is to remove the damage from earlier grinding process and to produce a transparent surface. In general, a piece of glass is pressed against a polishing pad and the two are moved relative to each other (Fig. 12). Ceria replaced the use of iron oxides and other abrasives in the 1960's due to its ability to catalyse the hydration of silicon dioxide surfaces. This hydrated layer is softer than the glass and readily abraded. It is theorized that a $Ce^{+4}$ to $Ce^{+3}$ transition and the presence of surface cerium hydroxyl groups are the reasons for this catalytic effect [64 65]. The hydration steps are represented here:

Equation 5. $-SiO_2 + H_2O \rightarrow -Si-OH \rightarrow -Si-O^- + H^+$

Equation 6. $-Si-O^- + Ce-OH <\rightarrow -Si-O-Ce-- +OH^-$

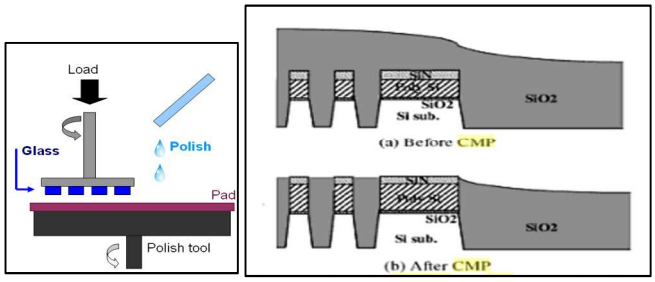


Figure 12. Chemical Mechanical Polishing (a) of a glass element and Chemical Mechanical Planarization (b) of silicon wafer showing shallow trench isolation of the SiO2 overgrowth. Figure kindly provided by Mark Mayton.

It was estimated that in 2011 that 23,600 metric tons of ceria containing polishing compounds were used worldwide to polish a variety of glass surfaces including mirrors, architectural glass, decorative crystals, flat panel displays, hard disk drives, precision optics and semiconductors [66]. For this use, ceria particle sizes range between 1 and 3 microns and the dominant production process involves precipitation in the presence of additives followed by calcination and milling.

Chemical Mechanical Planarization (Fig. 12b) of semiconductor wafers is a vitally important process by which $SiO_2$ is removed in varying stages over the active transistor region [67 68]. This process, which is called shallow trench isolation, (STI) enables the stacking of ten or more device layers, thereby increasing on-chip transistor density and computing/storage capability. The mechanism of action for ceria is similar to that seen in optical lens polishing but very high atom purity (>99.99%) is required to avoid un-intentional silicon doping effects. Typically, 100 to 300 nm particles are used for these applications.

As the line spacing between features on the semiconductor devices continues to shrink (68 nm in 2007 declining to 16 nm in 2018) there is a strong demand for smaller polishing particles which are less

likely to scratch surfaces and leave less residue on the wafer surfaces [69].

While the focus to this point has been on nanoscale $CeO_2$ chemistry, the ability to translate these results into commercial products can be a separate challenge. These challenges are discussed in two recent market research reports, Future Markets reported in Keller et al. [70] and SRI reported by the European Commission's staff [71]. It is estimated that the global production for nanoceria is 10,000 metric tons (mt) yearly. During discussions at the SNO nanoceria workshop, however, we could only identify much lower quantities: 170 mt/y for chemical mechanical polishing/planarization (CMP); 75 mt/y for European diesel additives and 100 mt/y in the French nanomaterial registry [72]**.** To reconcile these estimates, it would appear that there are in fact two markets. One for $CeO_2$ where the particles are supplied as an ingredient in powder or dispersion form, and one for $CeO_2$ where the particle is formed during manufacture, but supplied as a soluble metal salt in liquids. This market is likely the automotive catalyst market. The smaller ingredient market is the subject of chemical registration and labelling laws; the larger product market likely contributes to environmental CeO2 releases.

The fate of nanoceria in the environment and environmental pathways by which human and ecological receptors are exposed was discussed at greater length at the SNO Workshop.

Similarly, the end-use markets place specific performance requirements on particle suppliers. The diesel additive and automotive catalyst markets, described below, require specific combustion conditions, which have severe price restrictions. For both, the high temperature conditions essentially activate the particle surface, which means that variability in the particle manufacture is accepted if the cost is low. For CMP, however, surface chemistry is paramount, as the product will be provided in a complex chemical formula with additives. Performance occurs in an aqueous colloid at ambient temperatures. Minimal contamination and well-controlled, uniform production processes are required and costs may be higher.

**Catalytic Processes: Syngas, Catalytic Converters, Diesel Particulate Filters and Fuel Borne Additives**

Synthetic gas, or Syngas, [73] a commercially important and valuable material, has uses in the synthesis of ammonia for fertilizer, hydrocarbon production by Fisher Tropsch chemistry [74], desulfurization of fuels and cracking high molecular weight organics into smaller molecular weight fractions, to name but a few. Methane steam reforming [75] is the major commercial source of synthetic hydrogen ($H_2$). This reaction takes place in the temperature range 730 °C to 1100 °C and uses water to partially oxidize methane to carbon monoxide and hydrogen. Ceria can be used as a catalyst, (Eq. 7 and 8) to promote this reaction at even lower temperatures than currently employed [76] by doping with precious metals such as Pd [77] or even transition metals such as Ni [78].

Equation 7. $CH_4 + CeO_2 \rightarrow Ce_2O_3 + CO + 2H_2$

Equation 8. $Ce_2O_3 + H_2O \rightarrow 2\,CeO_2 + H_2$

In the process known as the partial oxidation of methane, regeneration of ceria (Eq. 8) can be accomplished with oxygen as shown is Eq. 9.

Equation 9. $Ce_2O_3 + ½\ O_2 \rightarrow 2CeO_2$

The water gas shift reaction (WGS) [79] involves the complete oxidation of carbon monoxide to $CO_2$ using water with the subsequent liberation of hydrogen. There are numerous literature reports of ceria and doped ceria catalysing the WGS reaction [80-82]. Eqs. 10 and 11 show how ceria can also serve as a catalyst for this reaction.

Equation 10. $CO + 2CeO_2 \rightarrow Ce_2O_3 + CO_2$

Equation 11. $Ce_2O_3 + H_2O \rightarrow 2CeO_2 + H_2$

These reactions demonstrate the gross features of the chemistry with efficiency enhancements and reduction to economies of scale being provided by precious metal doped substrates.

Perhaps no other compositions of matter have produced as profound a positive benefit on the state of human health as ceria and other catalysts in their use in automotive catalytic converters (ACC) and diesel particulate filters (DPF). The 1970 EPA Clean Air Act mandated exhaust emission reduction for on-road vehicles that were implemented by automobile manufacturers in 1975 for gasoline powered automobile engines and in 2007 for diesel powered vehicles. Carbon monoxide emissions from automobiles decreased by an estimated 76.3% relative to the pre catalyst 1975 levels and unintentional motor vehicle–related CO death rates declined from 4.0 to 0.9 per 1 million person-years (an estimated decline of 81.3%). This resulted in the savings of an estimated 11,700 lives [83]. The reduction in fine particle and ozone pollution alone in just 2010 is estimated to have prevented over 150,000 cases of premature mortality, 130,000 of heart attacks and 1.7 million asthma attacks. These numbers are expected to grow by 50% in another decade [84]. Additionally, population health improvements were aided by the removal of the toxic substance tetra ethyl lead from gasoline as this compound poisoned the catalytic converter. Further increases in these health benefits will accrue going into the future since 2/3$^{rd}$ of all US oil is consumed in transportation and a 50% increase in oil consumption is predicted by 2025[85].

Ceria's role in ACC and DPF emissions control technology is that of a three way catalyst whose oxidation and reduction efficiency is considerably enhanced when decorated with the precious group metals, Pt and Rh [86 87].

The following three processes define three-way ceria catalytic function [88]:

1. Unburned hydrocarbons are oxidized to carbon dioxide and water.
2. Carbon monoxide is oxidized to carbon dioxide.
3. Oxides of nitrogen are reduced to diatomic nitrogen and oxygen.

The concept of bringing the catalytic converter into the combustion chamber to increase combustion efficiency, improve fuel economy, and reduce exhaust emissions is the concept behind the use of ceria and ceria like materials as a fuel additive. Fuel efficiency improvements of 5-8 % along with concomitant 10-15% reductions of unburnt hydrocarbon, carbon monoxide and particulates have been reported with the use of Envirox®, a ceria-based product [89 90]. Significantly, no change in the soot particulate size-frequency distribution was reported with the use of the additive. A platinum/ceria combination called Platinum Plus® was at one time marketed by Clean Diesel Technologies. Rhodia has a fuel additive product line called Eolys® , which is an iron and ceria nanoparticle formulation used for the regeneration of diesel particulate filters. Normally, these diesel fuel additives are dosed into the fuel in the 5 to 25 ppm range [91]. Fuel additive volumes for Envirox® in the U.K. are estimated at a maximum of 11 metric tons per annum (mtpa) with 240,000 cars, 1,000 London buses and 8,000 Stagecoach buses. Extrapolated to the entire European Union these fuel additives are a very small market of approximately 75 metric tons per annum. Finally, Cerion LLC manufactures and markets a 2.5 nm nano-composition of cerium and iron called $GO_2$® that has been well characterized [7, 31] and is enjoying commercial success in the superyacht space (Go2 Global Yachting) primarily for the remediation of diesel generator-produced soot.

**Ceria Applications in Solid Oxide Fuel Cells (SOFC) and Other Electrochemical Devices**

SOFCs are extremely efficient (85%) generators of electricity and are a logical and attractive choice to replace the inefficient process of fossil fuel combustion (33%) [92]. SOFC have three major components; an anode, an ion conducting electrolyte and a cathode [93] (see Fig. 13).

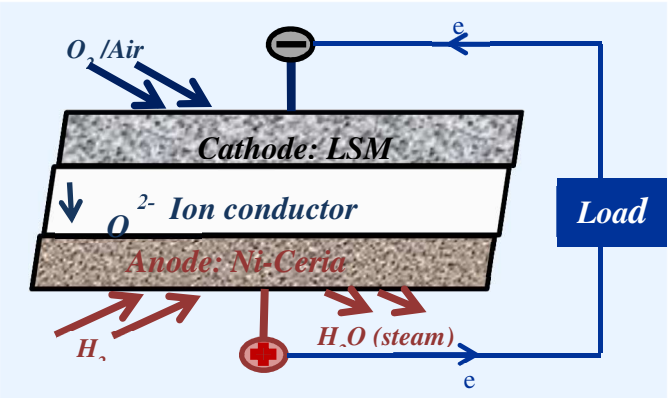


Figure 13. A SOFC schematic diagram comprising the basic elements: Cathode, Electrolyte and Anode driving an external load. LSM= lanthanum strontium manganite. Figure kindly provided by Aniruddha Kulkarni.

A fuel such as $H_2$ or a hydrocarbon [94] is supplied to anodic side and an oxidant, typically air, is supplied to the cathode. Oxygen is reduced to the ion ($O^{2-}$) and migrates across the solid electrolyte to react with $H_2$. The solid electrolyte allows transport of only oxygen ions, while the electrons released during the oxidation are available to drive an electrical load. Ceria compositions may be components of both the anode (normally Ni based cermet) and cathode (normally lanthanum strontium manganite, LSM). Ceria compositions (Sm, Gd, Y doped ceria) [95] are preferred as the electrolyte in the so-called intermediate temperature SOFC (ITSOFC) systems which operate in the temperature range of 500-600°C. These lower ceria-enabled operating temperatures, provide longer SOFC lifetimes, high efficiencies (90%) and are easier to manufacture as they require less exotic materials (https://www.sofcwg.org/motivation.php) than cells using yittria stabilized zirconia operating at 800 °C.

SOFCs are beginning to take their place in stand-alone installations. In 2012, 45,700 fuel cells were manufactured and shipped (including, but not exclusively ceria-based cells) which is twice the number in 2011 [96].

Ceria-based materials finds several applications in other electrochemical systems like gas separation membranes, ceramic oxygen generators (COG), solid electrolyte electrolysers and gas sensors. Application of nanoceria in place of micro-ceria improves the target properties in all of these applications. For example, response time of a thick film resistive oxygen sensor was found to decrease by an order of magnitude when the particle size of ceria was changed from 2μ to 100 nm[97]. Recently it has been shown that nanoceria sensors have faster response and recovery times in odor detection ($H_2S$ and $CH_3SH$ ) than commercially-available ZnO thick film sensors.[98]

**Ceria Applications in Everyday Life**

Interestingly, we encounter many ceria-based technologies in our everyday lives without actually recognizing this fact. These include; decolorization of glass's UV absorption (300-400nm). This process is used in glassware display cases, in passivating titania radiation resistant glass and for the protection of photosensitive glasses, optical coatings, and (formerly) TV picture tubes. Compact fluorescent lighting uses ceria as the optical sensitizer for the 245 nm Hg emission that photoexcites the fluorescent material in these devices. Finally, ceria is used as a component of the interior coatings of self-cleaning ovens.

## Potential Future Applications

In this section we will discuss three future areas of ceria and ceria-like materials that bear directly on the environment, future energy needs and human disease. The therapeutic potential of ceria will be discussed at length both to its emerging importance and as it provides an opportunity to explore the mechanisms of this redox material now working at physiological temperatures. This discussion will build upon concepts already discussed. Additionally, we provide additional insight into the pro- and anti-oxidant properties of nanoceria in the review by Grulke and colleagues in this themed collection [114].

**Chemical Looping Combustion**

Chemical looping combustion (CLC) employs oxygen from a metal oxide carrier MeOx, instead of ambient air for fuel combustion [99]. The oxygen carrier (usually an iron oxide) is circulated between two fluidized beds-an air reactor and a fuel reactor.

During the combustion cycle an oxidized carrier reacts with the hydrocarbon fuel:

Equation 12. $2\ MeOx + C \rightarrow 2Me + CO_2$

Equation 13. or $MeOx + H_2 \rightarrow MeOx + H_2O$

In the regeneration cycle the oxygen carrier is re-oxidized in the air reactor:

Equation 14. $2Me + O_2 \rightarrow 2\ MeOx$

The oxidized carrier is separated from the $N_2$ and fed to the fuel reactor. As a result, a relatively pure stream of $CO_2$ is produced that is immediately ready for storage. Other advantages include low to no $NO_x$, facilitation of Hg removal and improved thermal efficiency over direct air combustion. Nano iron oxide and variants including ceria in the iron formulation have been proposed to address some of the CLC limitations especially that of the need for enhanced reactivity and extended oxygen carrier lifetime

**Photolytic and Thermolytic Water Splitting**

With the increasing emphasis on replacing hydrocarbon fuels as society's main energy source and reduction of green house gas emissions, hydrogen has emerged as a leading candidate for the fuel of the future [75].

Efficient visible-light photo catalytic water splitting by various materials such as titanium dioxide, iron oxide and ceria is currently a very active area of research globally. Typically, very small quantities of a precious metal such as gold or platinum are used to decorate these functionalized nanoparticles to enhance photo-efficacy for the photo catalytic production of oxygen. As an example, Primo et. al. [100] describe one weight percent decorated gold supported 5 nm ceria nanoparticles to generate oxygen from water using visible light with an efficiency that is greater than that of the standard material $WO_3$. In another example, Kundu et. al. [101] use a platinum/cerium modified TiO2 electrode to split water again using visible light. The authors claim that this system is almost seven times more efficient than the standard $WO_3$ catalyst.

The direct production of hydrogen by high temperature thermal processes has been the concerted focus of W. C. Cheuh [102]. In a series of papers he describes a process that concentrates sunlight by a factor of 1,500 using an array of focusing mirrors [103]. The sunlight heats the cerium oxide to 1,500 °C, driving out its oxygen. As the reduced ceria is cooled, steam is then fed to the reactor reoxidizing the ceria while liberating hydrogen. The hydrogen can be collected, and the entire process repeated. In a further evolution of his work, Cheuh is trying to make cerium oxide–based hydrogen generation work at 500 °C, thereby obviating the need for exotic and expensive alloys required by the higher temperature process.

**Ceria as a Therapeutic Agent**

Reactive oxygen species (ROS), or oxygenated free radicals such as superoxide, $O_2^-$ and peroxynitrite $ONOO^-$, are produced as normal by-products of cellular metabolic pathways, but are also thought to play a major role in the pathogenesis of many diseases. In addition to their normal roles as secondary messengers in cell signalling and as immune activators, excess ROS can lead to deleterious effects by damaging DNA, proteins and lipids and thereby adversely effect their normal operation. The perceived ability of nanoceria to limit these deleterious reactions has inspired increasing research [104] [105] [106] [107] [108] resulting in a better understanding of the biological outcomes of administered cerium dioxide nanoparticles. Initial studies utilized *in vitro* cell culture models, while more recent work has been performed *in vivo* in relevant disease models, as discussed in detail at the SNO ceria workshop. It was principally noted at the SNO ceria workshop that the biological studies involving nanoceria exhibit significant variability and conflicting outcomes.

The use of nanoparticles in general, and specifically nanoceria, to beneficially modulate excess ROS concentration is not without it own set of biological issues and complexities [109] [57]. Aside from the possible perturbation of homeostatic cellular ROS activities, there are also possible attendant toxicological effects that likely depend upon mode of nanoceria administration in addition to the particulars of particle synthesis and stabilization. This important and complex subject is treated in much greater detail in a review in this themed collection by Yokel and colleagues [115].

The mechanisms by which a ceramic catalyst, whose normal chemical action is usually associated with the high temperatures (>450°C ) beneficially operate at physiological temperatures (37 °C) is presently unclear. It is generally agreed that ceria must perform two functions: one, to act to oxidize superoxide (a so called superoxide dismutase (SOD) mimetic), and secondly, to act as a hydrogen peroxide catalase to destroy peroxide. However, the exact reaction details describing how these activities occur are, presently, very much open to debate. As we shall see, nanoceria acting as a SOD mimetic and peroxide catalase requires it to be both a pro- and an anti-oxidant depending on the chemical specie that is being oxidized or reduced. A separate review in this themed collection addresses the conditions leading to these diametrically opposed behaviours [114]. The following discussion is intended to propose a mechanistic set of equations that might reconcile these behaviours while making a logical connection to the physical concepts previously discussed in this introductory paper.

There are two schools of thought on the SOD-mimetic, hydrogen peroxide catalase mechanism of ceria. The first is that the $Ce^{3+}/Ce^{4+}$ ions, interact directly to both neutralize (i.e. oxidize) superoxide and destroy peroxide. We will call this the ionic mechanism. The second school of thought is that both reactions proceed by oxygen vacancy creation and annihilation (filling), with the cerium ionic states

interchanging between plus three and plus four to accommodate the oxygen vacancy population.

Referring now to the ionic mechanism. The SOD mimetic component is thought to be favoured by an increase in the $Ce^{3+}/Ce^{4+}$ ratio [110] while the catalase component is favoured by a decrease in this ratio [111].

Rather than focusing on static ratios of ions, let us explore the thermodynamic reasonableness of the $Ce^{3+}/Ce^{4+}$ theory in greater detail by examining dynamic reaction chemistry.

One can write a complete and balanced set of equations for this mechanism, which is by no means unique, but exemplary:

Equation 15. $3Ce^{4+} + 3O_2^- \rightarrow 3Ce^{3+} + 3O_2$ $Ce^{4+}$ reduction

Equation 16. $Ce^{3+} + O_2^- + 2H^+ \rightarrow Ce^{4+} + H_2O_2$ $Ce^{3+}$ oxidation

These two steps (Eqs. 15 and 16) constitute the catalytic SOD-like dismutation reaction, while Eq. 17 represents the hydrogen catalase reaction.

Equation 17. $H_2O_2 + 2Ce^{3+} + 2H^+ \rightarrow 2Ce^{4+} + 2H_2O$

$Ce^{4+}$ regeneration and peroxide loss

For these equations it is implicitly understood that, as represented, a cerium ion in either the plus three or plus four state is not a free ion in solution but is the reactive atomic site that is part of an unspecified lattice structure.

We can further make the reasonable assumption that the disease pathology is somehow related to the excess superoxide that may be generated by hydrogen peroxide, as has been implicated in Parkinson's Disease. In reality, the excess of superoxide ion may be due to malfunctioning of the SOD1 and SOD2 enzymes, but it is mathematically more tractable to pose the equations as an excess of hydrogen peroxide:

Equation 18. $H_2O_2 + O_2 + 2OH^- \rightarrow 2O_2^- + 2H_2O$ super oxide formation

The free energy for the reaction, $\Delta G^0_{\text{reaction,}}$ as written in Eq. 18, is -369.1 kjoule/mole (-88.2kcal /mole), which is quite exothermic.

This net reaction for equations 15 through 18 is:

Equation 19. $H_2O_2 + 2O_2^- + 2H^+ \rightarrow 2H_2O + 2O_2$

Equation 19 demonstrates that the reaction both destroys superoxide (a SOD mimetic) and acts a hydrogen peroxide catalase (destroys hydrogen peroxide). Notice that ceria is absent in the net equation, which it must be if it is functioning as a catalyst.

As written, the net reaction (Eq. 19) is thermodynamically just slightly endothermic and would seem to be thermodynamically accessible at ambient physiological temperatures.

Equation 20. $\Delta G^0_{\text{reaction}} = 42$ kjoule/mole = 10.0 kcal /mole

Next, turning to the second mechanistic theory to explain the SOD and catalase-like behaviour of nanoceria, we focus on the role of the oxygen vacancy in destroying superoxide and rebalancing the $Ce^{3+}/Ce^{4+}$ couple [112]. L. Ghibelli and co-workers proposed an elaborate seven-step reaction sequence for the dismutation of superoxide, whose net reaction chemistry is:

Equation 21. $2O_2^- + 2H^+ \rightarrow O_2 + H_2O_2$

A separate six-step mechanism proposed for the catalase reaction leads to the reaction:

Equation 22. $2H_2O_2 \rightarrow O_2 + 2\,H_2O$

Equation 21 added to Equation 22 provides the net overall reaction (Eq. 23):

Equation 23. $H_2O_2 + 2O_2^- + 2H^+ \rightarrow 2H_2O + 2O_2$

Note that Eq. 23, representing the oxygen vacancy-driven mechanism is identical to Eq. 19 in the cerium ionic state cycling mechanism. Perhaps this should not be surprising given the interconnectedness of oxygen vacancy formation and destruction, and the required cycling between the two cerium atom redox states.

Finally, we would like to mention the possibility that surface ceria hydroxyl ions may play a role in the neutralization of superoxide. This thought is motivated by the discussion of role of ceria in CMP processes driven by ceria aquation [64]. Here, the surface cerium hydroxyl ions protonate superoxide forming hydroperoxyl radicals, which then undergo disproportionation in the following manner (Eq. 24);

Equation 24. $2\,HOO^- \rightarrow H_2O_2 + O_2$

It should be pointed out that the most emphatic support of an exclusive $Ce^{3+}$ mechanism and refutation of the vacancy mechanism was based upon the lack of an observed perturbation on vacancy formation as a function of samarium doping [113]. However, two serious issues arise from this assumption, as firstly, there was little evidence (XRD or otherwise) to support $Sm^{3+}$ incorporation into the lattice and secondly, one can make the logic-based argument that the lack of evidence of an effect is not the same as evidence for the lack of an effect.

Whether the two ionic states of lattice cerium react directly with superoxide and peroxide or the oxygen vacancy is the site of these chemical reactions with subsequent cerium ion charge accommodation may be more than just a matter of a semantic distinction without a difference. Substantially different chemical intermediates and kinetics will be involved that depend upon details of the mechanistic pathway.

The electronic behaviour and subsequent free radical reactions of hydrated ceria is still a very much open question, which, given the

 

promising medical applications of nanoceria is certainly deserving of much further investigation.

The foregoing discussion is, of course, a gross simplification of the real nanoceria behaviour especially in relevant biological systems where the plasma protein corona and other adsorbones can dramatically alter chemical behaviours. This complex subject was discussed at length during the workshop. It is our intention in exploring these mechanistic schemes to provide a skeletal framework for the animation of further discussion and experimentation.

## Conclusions

## Current Knowledge State and Summary

Nanoceria is an exceptionally versatile, commercially valuable catalytic material whose properties vary dramatically from that of the bulk material. Nanoceria's redox properties can be tuned by choice of method of preparation, particle size, nature and level of dopant, particle shape and surface chemistry. The two oxidation states of the cerium element in the lattice make possible the formation of oxygen vacancies which are essential to the high reactivity of the material, its oxygen buffering capability and thus its ability to act as a catalyst for both oxidation and reduction reactions. Ceria has important commercial utility in the areas of chemical mechanical polishing and planarization, catalytic converters and diesel oxidation catalysts, intermediate temperature solid oxide fuel cells and sensors. Its potential future uses include chemical looping combustion, photolytic and thermolytic water splitting for hydrogen production and as a therapeutic agent for the treatment of certain human diseases. We have seen that the method of synthesis, particle size, stabilizing corona, and purity dictate where it is used commercially. As Dr. Feynman suggested years ago, there still remains plenty of room at the bottom for exploration of nanoceria and its properties and uses.

## Nanoceria Knowledge Gaps

1. The question of material sustainability raised at the SNO nanoceria workshop, appears to be open, i.e. will there be enough of this rare earth element to sustain and perhaps grow its use in modern society?
2. A second issue that was expressed is that of making large-scale commercial quantities of uniform nanomaterial readily and economically available. This is one of the main stumbling blocks to the wide spread adoption and dissemination of nanotechnology in general. The practical engineering considerations of just which variables are needed to be controlled and to within what tolerances to achieve large-scale production, need to be understood.
3. It is very clear that not all nanoceria are created equal and that different nanoceria can have vastly different toxicological profiles. What are the synthesis parameters, particle size, stabilizers and other chemistries that affect these profiles?

## Research Recommendations

1. In order to better discriminate failed from successful ceria experiments and to understand the underlying reasons for these outcomes, especially with regard to biological systems, it was thought that some form of nomenclature or descriptor for a given ceria composition would be very useful as a unique identifier rather than just calling a material "nanoceria". Thus a unique label that could identify a composition of matter is a critical need.
2. Looking at the nature of the cerium salt precursor, the question was raised as to the uniqueness of the cerium nitrate salt (compared to other lanthanide nitrates). Certainly the nitrate salt is the most common and cheapest counter ion but nitrate is a good oxidizing agent (for $Ce^{3+}$ to $Ce^{4+}$ conversion) and it is reduced to NO, a pulmonary edema gas during high temperature synthesis. For biological applications, the choice of counter ion (gegen ion), can be important as for example in the use of the phosphate salt of cerium.
3. With regard to biological applications of nanoceria, the purity of the starting material should be fully characterized. Contaminant metals such as copper can dramatically affect the redox properties of nanoceria either beneficially or adversely.
4. Perhaps most intriguing is the question of the mechanism by which nanoceria appears to beneficially modulate excess reactive oxygen species (ROS). This mechanism or mechanisms needs to be elucidated. Do ROS interact directly with either the plus three or plus four state of the cerium atoms in the lattice (presuming the concept of integer ionic states is even valid) or does all the chemistry occurs in the oxygen vacancies (whose formation may be driven by the reduction of the plus four cerium state). It should also be pointed out that virtually all of our knowledge of the relative concentrations of the cerium states in the lattice comes from very high-energy, *in* vacuo XPS studies whose relevance to aqueous systems has been questioned. It is well known that these studies tend to overestimate the relative concentration of the $Ce^{3+}$ ion [27]. It would be helpful to have an alternative, less potentially damaging analytical technique to obtain an independent measure of this quantity.

## Acknowledgements

This article is a product of a workshop on nanoceria held November 2, 2013 at Fess Parker's Doubletree Resort, Santa Barbara, California which was made possible by financial support from the Sustainable Nanotechnology Organization; NSF grant CBET-1343638 to UCSB; and the Tracy Farmer Institute for Sustainability and the Environment, Department of Pharmaceutical Sciences, Office of the Vice President for Research, and Associate Dean for Research of the College of Pharmacy, University of Kentucky.

## Notes and references

[a] Cerion NRx LLC , US.
[b] Alfred University, US.
[c] CSIRO, Australia
[d] Spinnaker Cross, Inc., US
[e] University of Kent, UK
[f] Pennsylvania Bio Nano Systems, US

1. G. B. Haxel, J. B. Hedrick and G. J.Oris, *Rare Earth Elements-Critical Resources for High Technology*, USGS, 2002.
2. Molycorp Inc. , *A Lanthanide Lanthology*, Molycorp, Inc., 67750 Bailey Road, Mountain Pass, CA 92366, U.S.A., 1997.
3. Molycorp Inc., *Cerium_A Guide to its Role in Chemical Technology*, Molycorp, Inc., 1992.
4. R. D. Shannon, *Acta Crystallographica*, 1976, **A32**, 751-767.
5. Douglas A. Skoog, Donald M. West and F. James Holler, *Fundamentals of Analytical Chemistry (7th ed.)*, Harcourt Brace College Publishers, 1996.
6. A. Trovarelli, *Catalysis by Ceria and Related Materials,*, Imperial College Press, London, 2002.
7. R. K. Hailstone, A. G. DiFrancesco, J. G. Leong, T. D. Allston and K. J. Reed, *J. Phys. Chem. C* 2009, **113**, 15155-15159.
8. A. Patterson, *Phys. Rev.*, 1939, **56**, 978-982.
9. W. Tscharnuter, in *Encyclopedia of Analytical Chemistry*, ed. R. A. M. (Ed.), John Wiley & Sone Ltd., Chichester, 2000, pp. 5469-5485.
10. D. C. Sayle, S. Seal, Z. Wang, B. C. Mangili, D. W. Price, A. S. Karakoti, S. V. Kuchibhatla, Q. Hao, G. Mobus, X. Xu and T. X. Sayle, *ACS nano*, 2008, **2**, 1237-1251.
11. Q. Yuan, H. H. Duan, L. L. Li, L. D. Sun, Y. W. Zhang and C. H. Yan, *J Colloid Interface Sci*, 2009, **335**, 151-167.
12. D. R. Umananda M. Bhatta, Tamilselvan Sakthivel, Thi X. T. Sayle, Dean Sayle,Marco Molinari, Stephen C. Parker, Ian M. Ross, Sudipta Seal and Gunter Mobus, *J. Phys. Chem. C*, 2013, **117**, 24561-24569.
13. Satyanarayana V. N. T. Kuchibhatia, A. S. Karakoti, D. C. Sayle, H. Heinrich and S. Seal, *Cryst. Growth Des.* , 2009, **9**, 1614-1620.
14. Thi X. T. Sayle, Beverley J. Inkson, Ajay Karakoti, Amit Kumar, Marco Molinari, Gunter Mobus, Stephen C. Parker, Sudipta Seal and Dean C. Sayle, *Nanoscale*, 2011, **3**, 1823-1837.
15. Thi X. T. Sayle, Soumen Das, Umananda M. Bhatta, Gunter Mobus, Stephen C. Parker, Sudipta Seal and Dean C. Sayle, *Nanoscale*, 2013, **5**, 6063-6073.
16. Ajay S. Karakoti, Satyanarayana V. N. T. Kuchibhatla, Donald R. Baer, Suntharampillai Thevuthasan, Dean C. Sayle and Sudipta Seal, *Small*, 2008, **4**, 1210-1216.
17. X. F. Dean C. Sayle, Yong Ding, Zhong Lin Wang and Thi X. T. Sayle, *J. Am. Chem. Soc.*,, 2007, **129**, 7924-7935.
18. C. T. Campbell, *Science*, 2005, **309**, 713-714.
19. J. Kullgren, Ph.D. Thesis, Uppsala University, 2012.
20. S. F. Friedrich Esch, Ling Zhou, Tiziano Montini, Christina Africh, Paolo Fornasiero, Giovanni Comelli, and Renzo Rosei, *Science*, 2005, **309**, 752-755.
21. P. Dutta, S. Pal, M. S. Seehra, Y. Shi, E. M. Eyring, and R. D. Ernst, *Chem. Mater.*, 2006, **18**, 5144-5146.
22. S. Deshpande, S. Patil, KVNT Kuchibhatla and S. Seal, *Appl. Phys. Lett.*, 2005, **87**, 133113-133113.
23. Jean-Daniel Cafun, Kristina O. Kvashnina, Eudald Casals, Victor F. Puntes, and Pieter Glatzel, *ACS nano*, 2013, **7**, 10726–10732.
24. David Anthony Muller, Lena Fitting-Kourkoutis and Richard K. Hailstone, Cornell University, JumpStart 2009.
25. Annapaola Migani, Gerogi N. Vayssilov, Stefan T. Bromley, Francesc Illas and Konstantin M. Neyman, *J. Mater. Chem.* , 2010, **20**, 10535-10546.
26. Jing Zhang, Hitsohi Kumagai, Kae Yamamura, Satoshi Ohara, Seiichi Takami, Akira Morikawa, Hirofumi Shinjoh, Kenji Kaneko, Tadafumi Adschiri, and Akihiko Suda, *Nano Lett.*, 2011, **11**, 361-364.
27. Feng Zhang, Peng Wang, J. Koberstein,S. Khalid, Siu-Wai Chan, *Surf. Sci.*, 2004, **563**, 74-82.
28. Joachim Paier, Christopher Penschke and Joachim Sauer, *Chem. Rev.*, 2013, **113**, 3949-3985.
29. R. T. Suresh Babu, Talgat Inerbaev, Richard Day, Artëm E Masunov, Alfons Schulte and Sudipta Seal, *Nanotechnology*, 2009, **20**.
30. Alastair N. Cormack, Alfred University, ed., K. J. Reed, Powerpoint Presentation, 2011.
31. R. K.Hailstone, A. G. DiFrancesco, T. D. Allston, K. Parsiegla, and K. J. Reed, *J. Nanopart. Res.*, 2014, **16**, 2267-2278.
32. C. Sun, H. Li and L. Chen, *Energy & Environmental Science*, 2012, **5**, 8475.
33. H. I. Chen, H. Y. Chang, *Ceramics International*, 2005, **31**, 795-802.
34. Feng Zhang, Qiang Jin and Siu-Wai Chan *J. Appl. Phys.*, 2004, **95**, 4319-4326.
35. M. Hirano and E. Kato, *J. Am. Ceram. Soc.*,, 1999, **82**, 786-788.
36. M. Hirano and M. Inagaki, *J. Mater. Chem.* , 2000, **10**, 473-477.
37. K. Matsui, T. Kyotani and A. Tomita, 2002, **14**, 1216-1219.
38. M. Hirano and E. Kato, *J. Am. Ceram. Soc.*, 1999, **82**, 786-788.
39. L. C. Chunwen Sun, *Eur. J. Inorg. Chem.*, 2009, **2009**, 3883-3887.
40. J. M. Dowding, S. Das, A. Kumar, T. Dosani, R. McCormack, A. Gupta, T. X. Sayle, D. C. Sayle, L. von Kalm, S. Seal and W. T. Self, *ACS nano*, 2013, **7**, 4855-4868.
41. M. Niederberger, *Accounts of chemical research*, 2007, **40**, 793-800.
42. Christel Laberty-Robert, Jeffrey W. Long, Erik M. Lucas Katherine A. Pettigrew, Rhonda M. Stroud, Michael S. Doescher, and Debra R. Rolison *Chem. Mater.*, 2006, **18**, 50-58.
43. Stephane Abanades, Alex Legal, Anne Cordier, Gilles Peraudeau, Gilles Flamant and Anne Julbe, *J.Mater. Sci*, 2010, **45**, 4163-4173.
44. T. Matsui, K. Fujiwara, K. Machida, G. Adachi, T. Sakata, and H. Mori, *Chem. Mater.* , 1997, **9**, 2197-2204.
45. Y. J. He, B. L. Yang and G. X. Cheng, *Mater. Lett.*, 2003, **57**, 1880-1884.
46. S. Patil, S. C. Kuiry, S. Seal and R. Vanfleet, *Journal of Nanoparticle Research*, 2002, **4**, 433-438.
47. Swanand Patil, Sudipta Seal, Guo Yu, Alfons Schulte and John Norwood,, *Appl. Phys. Lett.*, 2006, **88**.
48. V. K. LaMer and R. H. Dinegar, *J. Am. Chem. Soc.* , 1950, **72**, 4847-4854.
49. Ya-Wen Zhang, Rui Si, Chun-Sheng Liao , and Chun-Hua Yan, Chao-Xian Xiao, and Yuan Kou, *J. Phys. Chem. B*, 2003, **107**, 10159-10167.
50. F. Zhou, X. Ni, Y. Zhang and H. Zheng, *J Colloid Interface Sci*, 2007, **307**, 135-138.
51. Karin L. Heckman, William DeCoteau, Ana Estevez, Kenneth J. Reed, Wendi Costanzo, David Sandford, James C. Leiter, Jennifer Clauss, Kylie Knapp, Carlos Gomez, Patrick Mullen, Elle Rathbun, Kelly Prime, Jessica Marini, Jamie Patchefsky, Arthur S. Patchefsky, Richard K. Hailstone and Joseph S. Erlichman, *ACS nano*, 2013, **7**, 10582-10596.
52. A. G. DiFrancesco, R. K. Hailstone, A. Langner and K. J. Reed, PCT/US2007/077545
53. Zhou Lu, A. J. Karakoti, Luis Velarde, Weina Wang ,Ping Yang, Suntharampillai Thevuthasan and Hong-fei Wang, *J. Phys. Chem. C*, 2013, **117**, 24329-24338.
54. Seung Soo Lee, Hulguang Zhu, Elizabeth Q. Contreras, Arjun Prakash, Hema L. Puppala and Vicki Colvin, *Chem. Mater.*, 2012, **24**, 424-432.
55. T. D. Allston, A. Langner, K. J. reed and L. Herder, US2010/0152077.
56. R. Feynman, American Physical Society, Caltech, California, 1959.
57. A. S. Karakoti, P. Munusamy, K. Hostetler, V. Kodali, S. Kuchibhatla, G. Orr, J. G. Pounds, J. G. Teeguarden, B. D. Thrall and D. R. Baer, *Surf. Interface Anal.* , 2012, **44**, 882-889.
58. Se-Woong Park, Wan-Jae Myeong, Jin-Soo Baik, Chang-Mo Chung, Kyu-Ho Song, US7754168 B2, July 13, 2010.
59. Takafumi Sakurada, Daisuke Hosaka, Kanshi Chinone, US8328893 B2, December 11, 2012.
60. Paul Gerard McCormick and Takuya Tzuzuki, US 6,503,475 B1 January 7, 2003.
61. Joke De Messemaeker, Stijn Put, Dirk Van-Genechten, Yves Van Rompaey, Daniël Nelis, Yvan Strauven, Gustaaf Van Tendeloo, US 12/866,485, Feb 24, 2011.
62. Stipan Katusic, Michael Kroell, Michael Kraemer, Stefan Heberer, Edwin Staab, Guenther Michael US 7553465 B2, Jun 30, 2009.

 

63. U. Gesenhues, *Solid State Ionics*, 1997, **101-103**, 1171-1180.
64. Minou Nabavi, Olivier Spalla and Bernard Cabane, *Journal of Colloid and Interface Science*, 1993, **160**, 459-471.
65. P. R. Veera Dandu, B. C. Peethala and S. V. Babu, *Journal of the Electrochemical Society*, 2010, **157**, H869-H874.
66. M. Mayton, *The Effects of the Price of Rare Earths on the Consumption of Polishing Compounds*, 2012.
67. Yukiteru Matsuia, Yoshlkuni Tateyamaa, Kenji Iwadea, Takeshi Nishiokaa and Hiroyuki Yano, *ECS Trans.*, 2007, **11**, 277-283.
68. Mahadevaiyer Krishnan, Jakub W. Nalaskowski and Lee M. Cook *Chem. Rev.* , 2010, **110**, 178-204.
69. International Technology Roadmap for Semiconductors, 2011 Edition, Front End Process, 2011.
70. Arturo A. Keller, Suzanne McFerran, Anastasiya Lazareva and Sangwon Suh, *J. Nanopar. Res.* , 2013, **15**, 1692-1694.
71. European Commission Staff, 2012. http://ec.europa.eu/nanotechnology/pdf/second_regulatory_review_on_nanomaterials_-_staff_working_paper_accompanying_com(2012)_572.pdf
72. M. Franck Eymery, Mmd.Aurelle Nlaudet, M. Anthony Cadene, M. Olivier Merckel and Mme. Nathalie Thieriet, *Elements issus des declarations des substances a l'etat nanoparticulaire*, Association european de libre-echange, 2013.
73. M. R. Beychok, *Process and evnironmental technology for producing SNG and liquid fuels,* , U. S. EPA 1975.
74. H. Schulz, *Advance Catalysis*, 1999, **186**.
75. George W. Crabtree, Mildred S. Dresselhaus and Michelle V. Buchanan, *Physics Today*, 2004.
76. N. Laosiripojanaa, and S Assabumrungrat, *Appl. Catal. B: Environmental*, 2005, **60**, 107-116.
77. X. Wang and R. J. Gorte, *Appl. Catal. A: General*, 2002, **224**, 209-218.
78. Jiahui Xua, Connie M. Y. Yeungc, Jun Nib, Frederic Meunierb, Nadia Acerbia, Martin Fowlesc, Shik Chi Tsanga, , *Applied Catalysis A: General*, 2008, **345**, 119-127.
79. Smith R. J., Muruganandam Loganthan, Murthy Shekhar Shantha *International Journal of Chemical Reactor Engineering*, 2010, **8**, 1-32.
80. Qi Fu, Howard Saltsburg, Maria Flytzani-Stephanopoulos, *Science*, 2003, **301**, 935-938.
81. Shido T. and Iwasawa Y., *J. Catal.*, 1992, **136**, 493-503.
82. T. Tabakova, Boccuzzi, F., Manzoli M. Sobczak J. W, Idakiev, V., Andreeva, D. A.,, *Appl. Catal. A*, 2006, **298**, 127-143.
83. Joshua A. Mott, Mitchell I. Wolfe, Clinton J. Alverson, Steven C. Macdonald, Chad R. Bailey, Lauren B. Ball, Jeanne E. Moorman, Joseph H. Somers, David M. Mannino, Stephen C. Redd, *JAMA*, 2002, **288**, 988-995.
84. U. S. E. P. A. Office of Air and Radiation, *The Benefits and Costs of the Clean Air Act from 1990 to 2020*, 2011. http://www.epa.gov/oar/sect812/prospective2.html
85. U. S. Energy Information Administration, *Short-Term Energy Outlook March 2014*, 2014.
86. H. C. Yao, and Y. F. Yu Yao, *J. Catal.* , 1984, **86**, 254-265.
87. R. H. Nunan J. , Cohn MJ ,and Bradley, SA, *J. Catal.*, 1992, **133**, 309-324.
88. J. Kaspar, P. Fornaserio and M. Graziani,, *Catal. Today*, 1999, **50**, 285-298.
89. Barry Park, Kenneth Donaldson, Roger Duffin, Lang Tran, Frank Kelly, Ian Mudway, Jean-Paul Morin, Robert Guest, Peter Jenkinson, Zissis Samaras, Myrsini Giannouli, Haris Kouridis and Patricia Martin, *Inhalation Toxicology*, 2008, **20**, 547-566.
90. Gareth Wakefield, Xiaoping Wu, Martin Gardener, Barry Park and Stuart Anderson, *Technology Analysis & Strategic Management*, 2008, **20**, 127-136.
91. A. C. Johnson and B. Park, *Environmental Toxicology and Chemistry*, 2012, **31**, 2582-2587.
92. International Energy Agency, *IES Statistics, Coal Information* ISBN 978-92-64, France, 2013.
93. U. S. Dept. of Energy, *Fuel Cells Handbook*, EG&G Technical Services Inc, 2013.
94. Park SD, Vohs JM, Grote RJ, *Nature*, 2000, **404**, 265-267.
95. Shaorong Wang, takehisa Kobayashi, Masayuki Dokiya, Takuya Hashimoto, *Journal of the Electrochemical Society*, 2000, **9**, 3603-3609.
96. FUELCELLTODAY, *The Fuel Cell Industry Review 2013*, 2013.
97. N. Izu, *Sensors and Actuators B* 2003, **93**, 449-452.
98. N. Izu, in *The 14th International Meeting on Chemical Sensors*, 2012.
99. Liang-Shih. Fan, *Chemical Looping Systems for Fossil Energy Conversions*, John Wiley & Sons, 2010.
100. Ana Primo, Tiziana Marino, Avelino Corma , Raffaele Molinari, and Hermenegildo Garcpromo, *J. Am. Chem. Soc.* , 2011, **133**, 6930-6933
101. S. Kundu, J. Ciston, S. D. Senanayake, D. Arena, E Fujita, D Stacchiola, L. Barrio, R. M. Navarro, J. L.G.Fierro, and J. A. Rodriguez, *J. Phys. Chem. C*, 2012, **116**, 14062-14070.
102. X. Ye, J. Melas-Kyriazi, Z. A. Feng, N. A. Melosh, W. C. Chueh, *Phys. Chem. Chem. Phys.*, 2013, **15**, 15459-154469.
103. William C. Chueh, Christoph Falter, Mandy Abbott, Danien Scipio, Philipp Furler, Sossina M. Haile, Aldo Steinfeld, *Science*, 2010, **330**, 1797-1801.
104. J. Colon, L Herrera.; Smith, J.; Patil, S.; Komanski, C.; Kupelian, P.; Seal, S.; Jenkins, D. W.; Baker, C.H. , *Nanomed-Nanotechnol.*, 2009, **5**, 225-232.
105. L. Kong, S Cai.; Zhou, S.; Wong, L.L.; Karakoti, A.S.; Seal, S.; McGinnis, J.F, *Neurobiol.Dis.* , 2011, **42**, 514-523.
106. C. K. Kim, T Kim, ; Choi, I.Y.; Soh, M.; Kim, D.; Kim, Y.J.; Jang, H.; Yang, H.S.; Kim, J.Y.; Park, H.K.; et al., *Angew. Chem. Int. Ed. Engl.*, 2012, **51**, 11039-11043.
107. A. Andreescu, M Ornatska; Erlichman, J.S.; Estevez, A.Y.; Leiter, J.C. , in *Fine Particles in Medicine and Pharmacy*, ed. E. Matijević, Ed., 2012, pp. 57-100.
108. A. Y. Estevez, J. S Erlichman, in *Oxidative Stress: Diagnostics, Prevention, and Therapy*, ed. S. Andreescu, American Chemical Society, Washington, D.C., 2011, pp. 255-258.
109. Andre Nel, Tian Xi, Lutz Mädler, Ning Li, *Science*, 2006, **311**, 622-627.
110. Eric G. Heckert, Ajay S. Karakoti, Sudipta Seal and William T. Self, *Biomaterials*, 2008, **29**, 2705-2709.
111. Talib Pirmohamed, Janet M. Dowding, Sanjay Singh, Brian Wasserman, Eric Heckert, Ajay S. Karakoti, Jessica E. S. King, Sudipta Seal and William T. Self, *Chem. Commun.* , 2010, **46**, 2736-2738.
112. Ivana Celardo, J. Z. Pedersen, Enrico Traversa and Lina Ghibelli, *Nanoscale*, 2011, **3**, 1411-1420.
113. Ivana Celardo, Milena DeNicola, Corrado Mandoli, Jens Z. Pedersen, Enrico Traversa and Lina Ghibelli, *ACS nano*, 2011, **5**, 4537-4549.
114. E. A. Grulke, K. Reed, M. J. Beck, X. Huang, A. Cormack and S. Seal, Environ. Sci: Nano, 2014, 1, DOI: 10.1039/C4EN00105B.
115. R. A. Yokel, S. Hussain, S. Garantziotis, P. Demokritou, V. Castranova, F. R. Cassee, Environ. Sci: Nano, 2014, 1, DOI: 10.1039/c4en00039k.